INFLUENCE OF INTERNAL ENERGIES ON OPTICAL PROPERTIES OF METHYL AMMONIUM LEAD TRIIODIDE THIN LAYERS

Research Article

i-PROCLAIM .my

Asia Pac. j. energy environ.

Cliff Orori Mosiori

Department of Mathematics and Physics, School of Applied and Health Sciences, Technical University of Mombasa, P. O. Box 92840, Mombasa, **KENYA**

*Email for Correspondence: corori@tum.ac.ke

Manuscript Received: 14 February 2022 - Revised: 7 April 2022 - Accepted: 1 May 2022

Abstract

In this study, various forms of energies affecting optoelectronic properties of CH3NH3PbI3 thin films are presented and explained experimentally and using theoretical models. Different concentrations of CH3NH3PbI3 solution were prepared, and thin films were deposited using spin-coating at a speed of 1000 rpm for 90 seconds and annealed at 100o C for about 60 minutes. Optical measurements were obtained, and the films were analyzed. The results showed that some properties, like absorption coefficients, ranged between 4.68073 - 22.19402×102 cm-1, dielectric constant between 4.10497 - 4.96329, and band gap between 1.6121 – 2.1642 eV. Various energies were determined, including transition energies, obtained as 1.742 eV, VE losses as 1.732 eV, average band gap at 1.723 eV, and SE losses at 1.714 eV. These values of internal energy had a significant direct influence on the optoelectronic properties of CH3NH3PbI3 and thus concluded that they could be used to provide initial useful information in designing and modeling hybrid perovskite optical devices.

Key words

Urbach Tail, Surface Energy Loss Function, Volume Energy Function, Electric Susceptibility, Inter-Band Transition Strength, Methyl Ammonium Lead Halides

INTRODUCTION

Hybrid perovskites are semiconductors. Hybrid perovskites are potential absorbers for several optical devices (Amgar *et al.*, 2016; Kim *et al.*, 2014; Vandewal *et al.*, 2018) and include methyl ammonium lead halide, represented by an empirical formula, $CH_3NH_3PbX_3$where X represents a halide atom. Much research is ongoing on methyl ammonium lead halides for photovoltaic and solar cell applications, whereby initial results point to outstanding optoelectronic properties for several optical applications. Specifically, $CH_3NH_3PbI_3$ exhibits itself as an exceptional photon absorber layer in solar cells (Vandewal *et al.*, 2018) and a few photovoltaic cell structures (Amgar *et al.*, 2016) within a direct band gap of 1.52eV. According to Shockley-Queisser theory (Arun *et al.*, 2015; Yuan *et al.*, 2016), it exhibits a total absorption flux potentially of above 80% in a single diode junction application.

Further still, as an absorber layer at an appropriate thickness, it shows the potential of having very high absorption coefficients below its band gap (Vandewal *et al.*, 2018) making it an excellent potential candidate for single junction solar cells in tropical African regions. Many optoelectronics properties are influenced by different types of internal energies present in a perovskite material as they significantly influence fundamental intrinsic mechanisms unique to perovskite materials. These internal energies include band gap energy (Gogoi & Schmidt, 2016), weak absorption tail energy, surface energy function; volume energy function, and Urbach energy.

Among these energies, several theoretical approaches have been employed to determine band gap energy (Vandewal *et al.*, 2018), binding power of occupied states (Edoardo *et al.*, 2016), spin-orbit coupling energy (Men´endez-Proupin *et al.*, 2014), and even Quasi-elastic neutron scattering point (Edoardo *et al.*, 2016), but their finding is still under debate. Further still, even values by expensive methods like Density functional theory (DFT) (Mattoni *et al.*, 2016), *ab initio*

calculations (Edoardo et al., 2016), Density-based schemes, and Green's function-based schemes remain debatable. However, recent inexpensive approaches like Local-Density Approximation (LDA) (Edoardo *et al.*, 2016; Mattoni *et al.*, 2016), semi-local GGA and the Perdew BurkeErnzerhof (PBE) tend to agree on band gap energies only if they ignore the influence and the energy contributions from Urbach energy (E_U), Weak Absorption Energy (WAT), Surface Energy Function (SELF) and Volume Energy Function (VELF), Activation energy (E_{act}) and Spin–Orbit Coupling Energy (SOCE). In hybrid $CH_3NH_3PbI_3$ perovskites crystals, deviations to determine internal energy is attributed to the tetrahedral structure and heterogeneous composition sensitivity of the crystals, the underestimation of binding energy of the occupied states (Kholmirzo *et al.*, 2015) and the splitting that occur in the occupied and unoccupied orbitals.

The good news is that different computational methods (Edoardo et al., 2016) have yielded similar band gap values. However, they fail to provide helpful information on the other associated internal energies leaving room to speculate on their influence on band dispersion, molecular dynamics (Kholmirzo *et al.*, 2015), preferential orientations or re-orientations, tilting, rotating, and crystal re-alignments (Amgar *et al.*, 2016). A detailed understanding of the various internal energies and how they influence the optical and electrical constants of $CH_3NH_3PbI_3$ films may influence the orientation research on perovskite in the next generation. It is, therefore, essential to investigate methyl ammonium lead tri-iodide perovskites film energies as this may provide useful information to understand its optical mechanisms and properties. In this paper, various energies affecting $CH_3NH_3PbI_3$ are determined and presented.

THEORY

A fundamental thin film intrinsic semiconductor property is band gap energy (Gokmen *et al.*, 2013). Its determination involves a process of exciting electrons (Lindblad *et al.*, 2015; Mariona *et al.*, 2015; Mattoni *et al.*, 2016; Men´endez-Proupin *et al.*, 2014; Nadim *et al.*, 2016) from a valence (VB) to the conduction (CB) band with a crystal. Urbach energy is another intrinsic property (Gogoi & Schmidt, 2016). It adds a small amount of energy that influences the relationship between total photon absorption flux and the nature of the material (Gokmen *et al.*, 2013). It also affects the length of the Urbach tail. It ends up influencing the absorption spectra by creating three unique, distinguishable absorption spectral regions: (1) a region of *weak absorption* that arises due to the presence of defects and inclusion of impurities (Lien *et al.*, 2015; Mattoni *et al.*, 2016; Sadhanala *et al.*, 2015; Simon *et al.*, 2015); (2) an *absorption edge* which is a region associated with the presence of disorders that affect band gap energy; and (3) an *absorption* region associated with crystallinity. The Inter-band transition strength (J_{cv}) is another energy-related parameter that accounts for dipole selection that influences electron transitions in perovskite films. It can be used to determine the probable occurrence that an electron can have enough energy to transit between a filled VB and an empty CB since this is a functional component of a material's dielectric constant related as (Arun *et al.*, 2015):

$$J_{CV} = \frac{4\pi m_o^2}{e^2 h^2}\frac{E^2}{2}\left(\varepsilon_1 + i\varepsilon_2\right) \quad (1)$$

in which m_o is the mass of transiting electron, E is the energy carried by the photon, e is the charge constant of an electron, and h is the constant derived by Planck. The component $\left(\frac{4\pi m_o^2}{e^2 h^2}\right)$ is pre-factor approximated to 8.289 x 10^{-3} eV^{-2} with units of cmg^{-3} (for *computing purposes only*).

Surface energy loss functions (SELF) is another internal energy function that can describe transition energy in a thin film and show whether a film is thin or in bulk by relating as:

$$SELF = -\mathrm{Im}\left(\frac{1}{\varepsilon+1}\right) = \frac{\varepsilon_2}{\left[(\varepsilon_2+1)^2+\varepsilon_2^2\right]} \quad (2)$$

where the symbols ε_2 and ε_1 refer to the imaginary and real constants. When both exhibit a smooth trend shown by their SELF functions, they imply that there is a uniform thin film surface present. The surface, therefore, is relatively and uniformly smooth. Electrons traversing a thin layer form a reciprocal quantity of its imaginary dielectric constant and therefore, the Volume energy function (23) can be used to explain the rate of energy electrons loss as they move in a film. It accounts for the reciprocal part of the sum of the dielectric constants. A significant deviation in C losses between films signals an increase or presence of slightly more defects or non-uniformity in the thickness of the films. VELF directly relates to dielectric function by the relation:

$$VELF = -\mathrm{Im}\left(\frac{1}{\varepsilon}\right) = \frac{\varepsilon_2}{\varepsilon_1^2+\varepsilon_2^2} \quad (3)$$

The sum of effective internal film energies influences electric susceptibility (χ_e), a dimensionless constant that controls film polarization as it responds to any externally applied electric field.

METHODOLOGY

Substrate Preparation

About 3 × 3 cm^2 active dimensions of glass substrates were cleaned according to the procedure by Wei *et al.* (2018). Each substrate was well scrubbed in warm de-ionized water having a neutral soap solution, and after cleaning, they were rinsed in flowing de-ionized water. They were finally dried by exposing them to spinning air and later place in an oven at 150° C for 4 minutes after which, they were cooled to room temperature before depositing a film on each of them.

Precursor Solutions

A powder mass of 10g of $CH_3NH_3PbI_3$ was accurately weighed with a precision balance. Enough N, N-Dimethyl formamide solvent was added, stirred with a magnetic stir-bar at room temperature, and the resulting solution was filtered using PTFE filters. Different concentrations ranging from 0.001 moles per liter to 0.012 moles per liter of $CH_3NH_3PbI_3$ precursor solution were prepared and used while fresh.

Depositing of the active layer

Before the spin coating process, the glass substrates were exposed to a temperature of 28° C that was pre-determined (*room temperature at the laboratory*) for about 5 minutes to attain uniform substrate temperature. Single Step Spin Coating technique was used. The spinning parameters were maintained constant and included a spin-coating speed of 1000 rpm, 90 seconds of spinning, and 100° C annealing temperature for 60 minutes. A VTC 200 spin coater model was used.

RESULTS AND DISCUSSION

It has interesting to investigate and study the optical properties of hybrid perovskite materials for many reasons. First, the optical properties of $CH_3NH_3PbI_3$ films have attracted an urge interest. In this work, they were investigated by studying the influence of the energies that characterize it as a potential material for optoelectronic devices. Second, a UV-VIS-NIR spectrometer measured the transmittances and reflectance of the films. Third, the Scout software simulations were performed using the simulated data, and numerical analysis was carried out. The following subsection presents and discusses the results obtained.

Dielectric constant

Figure 1 shows the variation of the actual dielectric constant in $CH_3NH_3PbI_3$ films. An increase in the dielectric constant with an increase in concentration was noted, as shown in Figure 2, which also shows the results obtained from simulation using the Tauc-Lorentz model of dispersion and fitting into the Lorentz oscillator model equation by substituting the Tauc density states. The results show that the fundamental dielectric constant exhibited exponential growth as the number of crystals in the films as concentration increased. This was a piece of evidence to attest that the actual dielectric constant is a function of concentration.

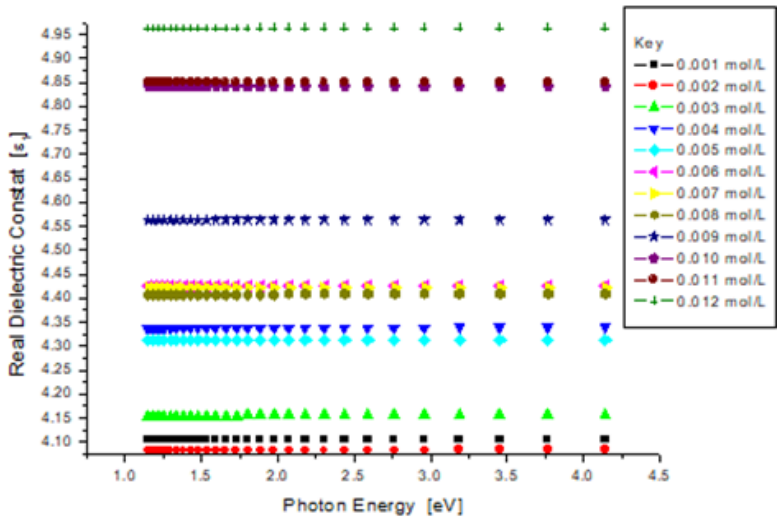

Figure 1: A curve for variation in fundamental dielectric constant vs. energy of the photon

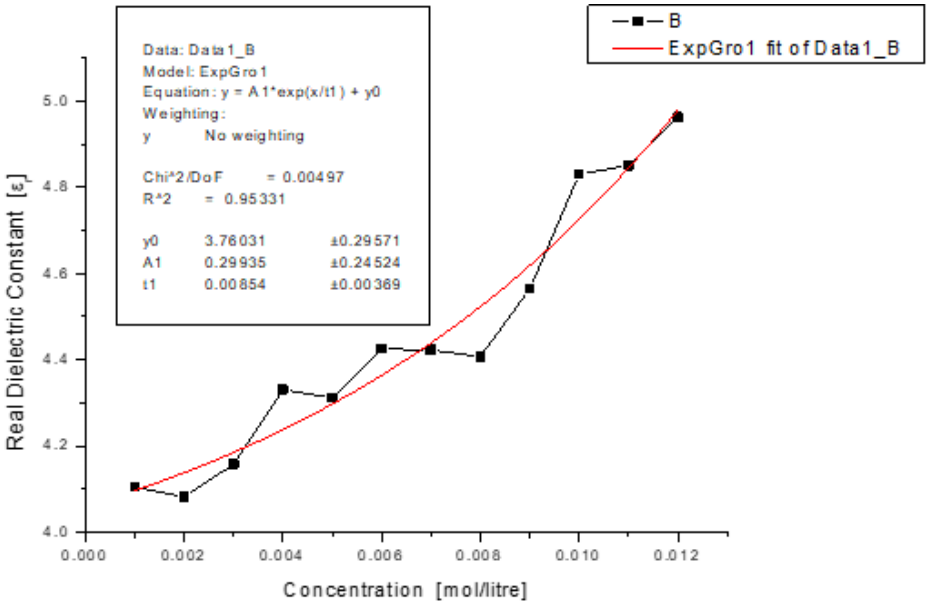

Figure 2: A plot of exponential growth fit on Real dielectric constant

The numerically analyzed fundamental dielectric constant was 5.7565, and the imaginary dielectric constant was 1.8504 $\times 10^{-5,}$ while the simulated natural dielectric constants ranged between 4.10497 to 4.96329 and the imaginary part ranged between 1.1115 $\times 10^{-5}$ and 2.3492 $\times 10^{-5}$ respectively. Similar observations have been reported elsewhere (Arun *et al.,* 2015; Chun-Sheng *et al.,* 2015; Edoardo *et al.,* 2016; Jun *et al.,* 2015; Kholmirzo *et al.,* 2015; Lindblad *et al.,* 2015; Mattoni *et al.,* 2016; Simon *et al.,* 2015; Wei *et al.,* 2018) that the dielectric constant is a function of concentration, and all agree with the dielectric constant variation recorded in this work. Knowing the dielectric constant of $CH_3NH_3PbI_3$ films forms one of the criteria for classifying it as a good insulation material, i.e., referred to as dielectric hybrid perovskite material, and whether it can be potential for other applications like capacitive materials. Since the dielectric constant is also known as relative permittivity, determining the permittivity ratio to that of its vacuum of $CH_3NH_3PbI_3$ films opens a window that allows the movie to be investigated for other optical device applications.

Absorption Coefficient and Extinction coefficient

Tauc Lorentz model was used to simulate the absorption coefficient, and the results are represented in Figure 3. This was built in the Scout software. Figure 3 shows that the absorption coefficient decreased with increasing wavelength and an increase in concentration and therefore formed a function of concentration depicting a normal dispersion as influenced by concentration. Figure 4 illustrated a Tauc Lorentz variation in absorption coefficient between 4.67 - 22.19 $\times 10^2$ cm^{-1} for 0.001mol/liter to 0.012 moles per liter concentrations, respectively, and compared to 8.15 $\times 10^2$ $cm^{-1,}$ which is a theoretical as documented by Edoardo *et al.* (2016). Figure 5 shows the extinction coefficient decreased with an increase in photon energy in all samples to about 1.5 eV (*wavelength, about 800 nm*), which increased with an increase in photon energy. The coefficients of extinction were relatively higher within the strong-absorption spectra and after that sharply decreased as wavelength increased to some turn-point photon energy approximated to be equal to band gap energy (approximately 1.56 eV) of $CH_3NH_3PbI_3$ films since extinction coefficient (k) depicts a measure of how a $CH_3NH_3PbI_3$ film absorbs photons at a particular wavelength.

Determining photon absorption capacity using the Tauc gap may help to inform another thin film measurement like spectroscopy to measure the concentration of a chemical in solution or to explain the source of certain specific optical parameters and even determine how they were generated from the precursor solutions. Figure 6 depicted a Tauc Lorentz fit on absorption coefficient in which a normal dispersion can be seen. The first principle calculation on extinction coefficient gave a value of 0.38085 compared to 0.34203 obtained by extrapolation. Though these values were relatively lower than those reported in the literature, similar trends in absorption and extinction coefficients have been reported that display a decrease in values to about 1.5 eV (Fan *et al.,* 2016; Gonzalez-Pedro *et al.*, 2014) followed by a uniformly prolonged increase (Sadhanala *et al.*, 2015; Yang *et al.*, 2017) to some higher absorption and extinction values. Hybrid perovskites exhibit a nonlinear absorption coefficient as a fraction of incident radiation absorbed per unit thickness of absorber. Knowing such a parameter is very significant in determining the mass absorption coefficient of $CH_3NH_3PbI_3$ films as this is obtained by dividing its linear absorption coefficient by the density of the $CH_3NH_3PbI_3$ films. In such cases, the amount of material and its mass can be determined and evaluated in terms of efficiency, cost and industrial viability.

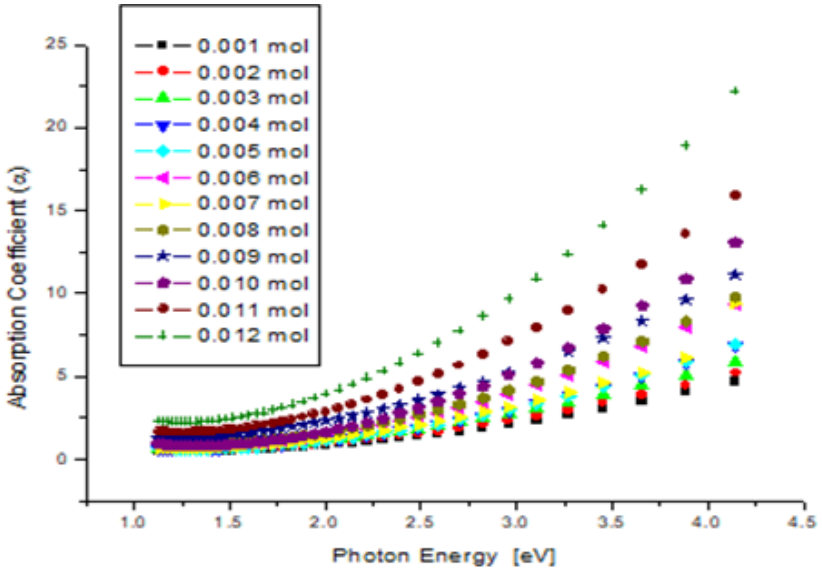

Figure 3: A Curve of coefficient of absorption vs. energy of the photon

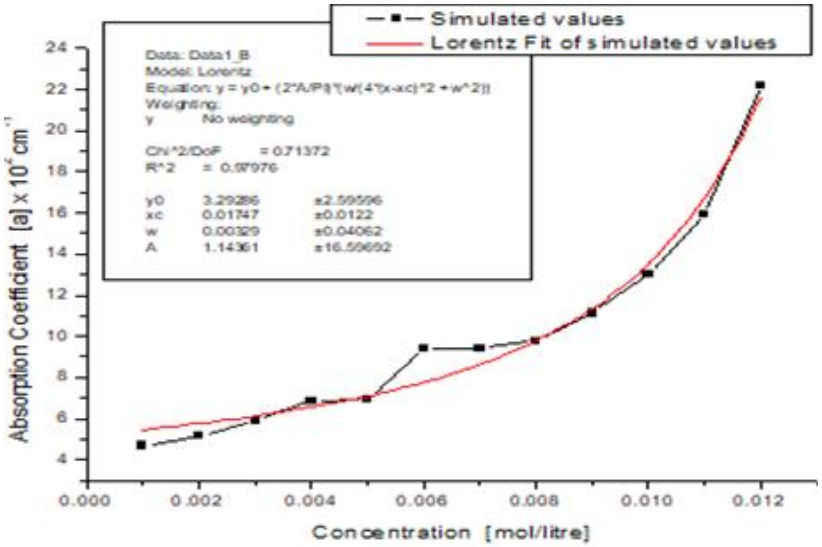

Figure 4: A plot of Tauc Lorentz Model fit on the absorption coefficient

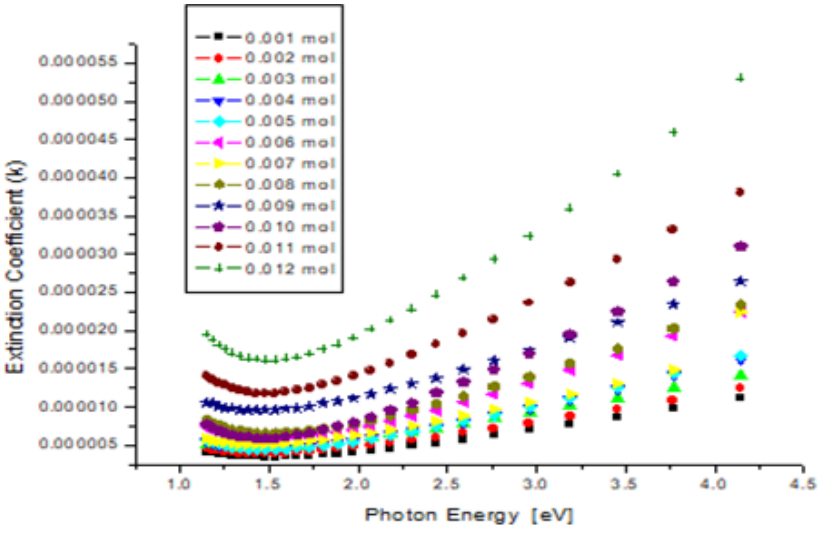

Figure 5: A plot of extinction coefficient against photon energy

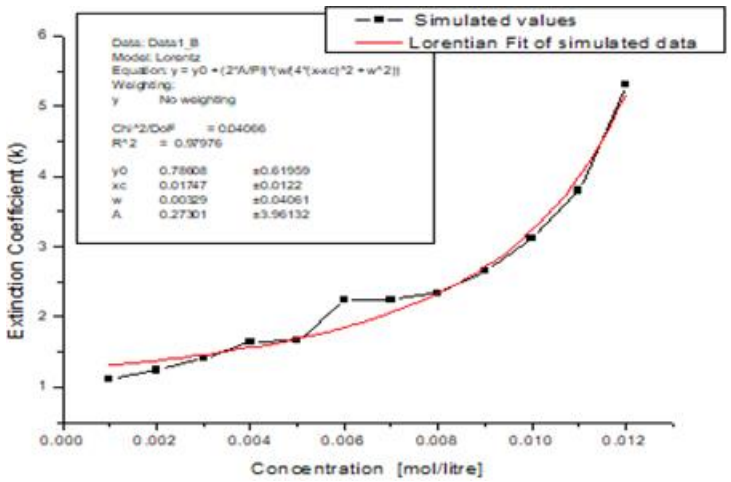

Figure 6: A plot of Tauc Lorentz fit of extinction coefficient

Optical band gap energy

This handy tool predicts the wavelength of an electromagnetic wave that the $CH_3NH_3PbI_3$ perovskite will absorb. In perovskites, it is well-defined energy between a valence band and a conduction band, and therefore, it is appropriate to call it the 'electron band gap' energy. The OJL model was used to simulate the band gap. The band gap is a susceptible intrinsic property according to the Moss Burstein effect as it responds to changes in concentration. Figure 7 illustrates the dependence of the band gap to attention in the film cover suggesting the energy increased with an increase in engagement. This was attributed to the rise of orbital bands that finally become overpopulated and merged due to increased crystal concentration. As a result, the gap energy (E_g) widens, obeying the Moss Burstein effect (Wei *et al.*, 2018; Yani *et al.*, 2016). A linear fit in fig 7 revealed a relatively more significant band gap than a theoretical value of 1.52 eV by an amount equivalent to 0.21 eV (*between* ~ 3.93 eV *and* ~ 5.43 eV). Finally, a band gap of 1.612 – 1.784 eV was obtained in this study with average gap energy of 1.721 eV.

Similar trends can be found in Men´endez-Proupin *et al.* (2014) while relatively larger values have been reported ranging from 1.671 - 2.183 eV (Jun *et al.*, 2015; Laura, 2016; Nagabhushanaa *et al.*, 2016; Sadhanala *et al.*, 2015; Simon *et al.*, 2015; Valerio *et al.*, 2016). However, most of these findings suggest that the presence of a single slope when determining the band gap reaffirmed that $CH_3NH_3PbI_3$ films are a direct allowed transition perovskite material. It should be noted that the band gap provides useful information in understanding how electromagnetic waves interact with hybrid perovskite materials. The band gap is a key intrinsic component in predicting the nature of interactions expected with its potential applications. A narrow gap absorbs longer wavelengths. It only requires a low amount of photon energy to initiate an electron to transit to the conduction band and vice versa for a large band gap that absorbs shorter wavelengths (UV region) due to the high photon energy required by the electrons to jump across a wide gap (Kim et al., 2014). It is, therefore very important to understand the significance of band gap energy in many phenomena associated with the hybrid perovskites and related nanomaterials.

Electric Susceptibility

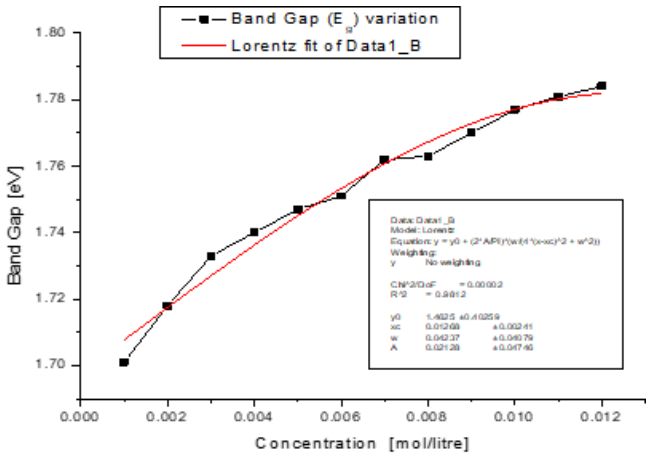

Figure 7: A plot of Band gap variation against concentration

Electric susceptibility by fee carriers was determined by plotting ε_r versus λ^2 plotted using the Wemple–DiDomenico, and Spitzer–Fan model equation (Gokmen *et al.*, 2013). The values obtained were then compared to concentration. It was noted that the importance of ε_∞ was almost practically constant throughout the spectrum (300 – 1100 nm), suggesting that the oscillation energy, E_0, can be approximated to $E_0 \approx 0.6E_g$. It also noted that the more significant this value was, the higher potential of the perovskite to get polarized in response to an external electric field. However, a non-uniform variation in electric susceptibility was noticed. This none uniform variation in electric susceptibility was attributed to the number of free carriers available that depend on the type of perovskite crystals and not on concentration. A similar explanation was given by Dalouji *et al.* (2017). Electric susceptibility influences permittivity, influencing many film abilities like capacitance for capacitors and speed of light for optical devices or films used for optical applications.

Figure 8 confirms that concentration contributes to the amount of electric susceptibility exhibited by a film and further suggests that when the dielectric constant of perovskite changes, the number of free carriers also changes, affecting free page electric susceptibility. This further confirmed that the Wemple–DiDomenico model that relates the energy to film polarization variations could imply that dielectric constant variation can be used to describe conductivity in these films. Furthermore, hybrid perovskites have been proposed to be used in many optical applications. Since electric susceptibility defines a quantitative extent to which an external electric field applied to a $CH_3NH_3PbI_3$ perovskite films causes polarization due to the slight displacement of their positive (anions which forms the organic part) and negative charge (cations which form the inorganic rotating and tilting or spin part) within the material, designing a unique optical system can rely of its variations or oscillating polarizability.

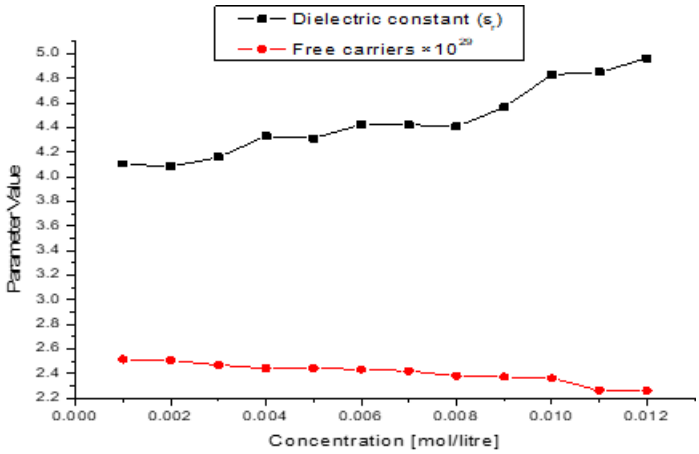

Figure 8: A plot of real dielectric constant versus square of wavelength (λ^2)

Urbach Energy

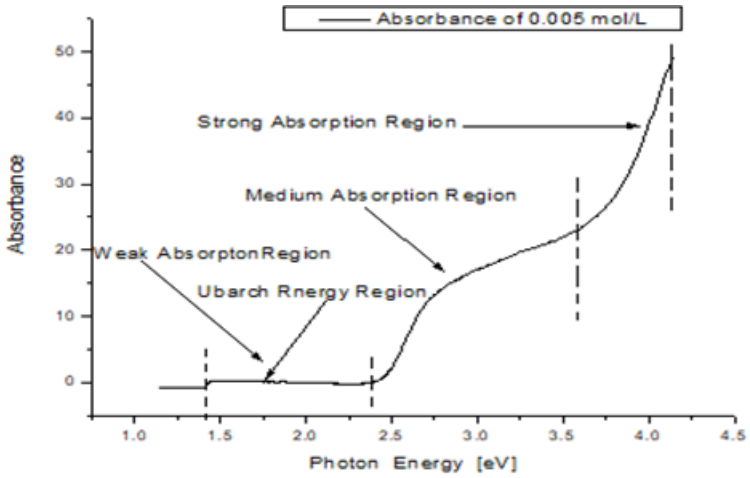

Figure 9: Plot of Absorption regions in a $CH_3NH_3PbI_3$ perovskite thin film

Figure 9 shows sections of the weak, medium, and vital absorption regions for $CH_3NH_3PbI_3$ thin films that were considered. Urbach energy (E_u) is the energy associated with the second region (*an absorption edge region associated with system disorders responsible for affecting band gap*). The Urbach energy was estimated by calculation. A curve of the

natural logarithm of *ln* (α) against *hv* was drawn and fitted with a straight line on its linear section. Its reciprocal was estimated as shown in Figure 10.

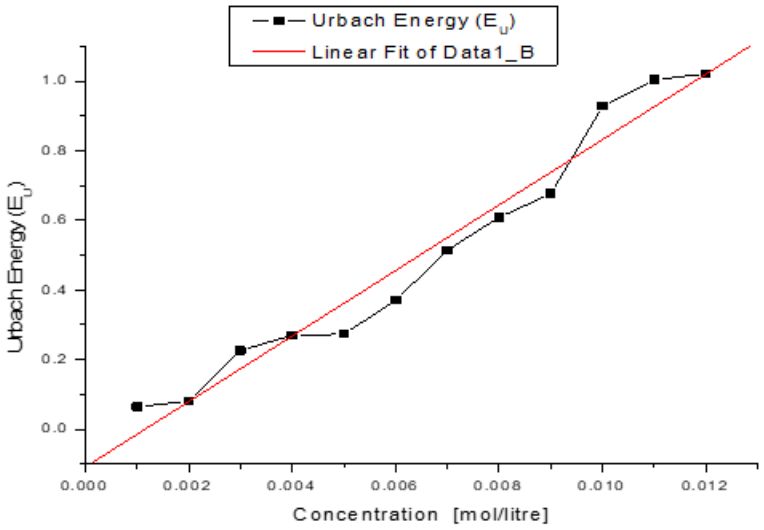

Figure 10: A plot of the variation of Urbach energy with concentration

Crystal of $CH_3NH_3PbI_3$ constantly undergoes some distortions and tilting resulting from the spatial variations in local bond coordination during distortion or rotation or tilting; Urbach energy also keeps changing depending on change in concentration. Such a change is attributed to internal solid fields arising from the introduced ionized PbI_3 rotating tetrahedral part (Kim *et al.*, 2014). However, some authors attribute this to temperature-induced disorders in $CH_3NH_3PbI_3$ crystals (Lee *et al.*, 2015) while others attribute it to short-range order changes that occur in $CH_3NH_3PbI_3$ crystals due to changes in concentration (Arun *et al.*, 2015; Lindblad *et al.*, 2015; Men´endez-Proupin *et al.*, 2014). Therefore, Urbach energy gives an idea of the amount of damage caused by bond changes in response to changes in concentration. In essence, the larger the Urbach energy, the greater the distorted news in its phonon states.

Surface and Volume Energy Loss Functions

SELF is a significant value that explains electron transitions in thin films. In this work, it was calculations using the finite Drude-Lindhard model equation and presented as shown in Figure 11. Figure 11 also indicates that each curve had a clear trend that was a function of concentration exhibiting an increase with an increase in concentration changes with an absolute value of 1.721 eV that was slightly lower than that of the importance of VELF held at 1.732 eV. This suggested that $CH_3NH_3PbI_3$ films were relatively thin with a relatively uniform surface that required confirmation from surface meter measurements. A similar trend has been reported (Nagabhushanaa *et al.*, 2016; Yuan *et al.*, 2016) elsewhere which enabled this result to suggest that a unique parameter was responsible for causing the slight variation the variation noted in each curve in Figure 11.

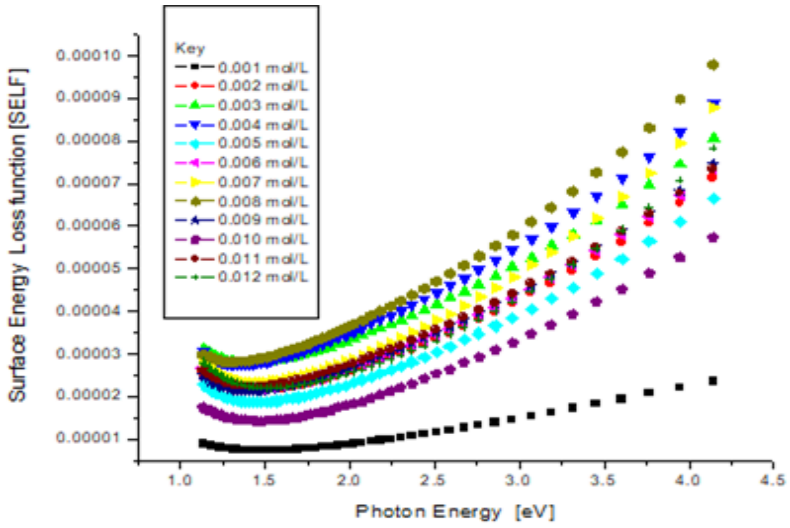

Figure 11: Plot of SELF against photon energy

This parameter was attributed to having a relationship with concentration and the probability that a free charge carrier (electron) can transmit. It suggested that SELF forms a significant parameter to consider when analyzing hybrid perovskites. Figure 12 also shows the variation of the volume energy loss function at different concentrations with photon energy. A unique interpretation that does not depend on concentration is noticed at lower and higher photon energies. Similarly, there is no clear trend in variation of VELF with attention or photon energy. This suggests that the $CH_3NH_3PbI_3$ films did not have a uniform volume or thickness, with a uniform surface with no highlands. Similar results were reported with similar attributes by Vandewal *et al.* (2018), and Yang *et al.* (2017). Few articles have attempted to determine VELF for hybrid perovskites (Vandewal *et al.*, 2018; Yang *et al.*, 2017; Yuan *et al.*, 2016), but those available display a similar trend to that shown in Figure 12.

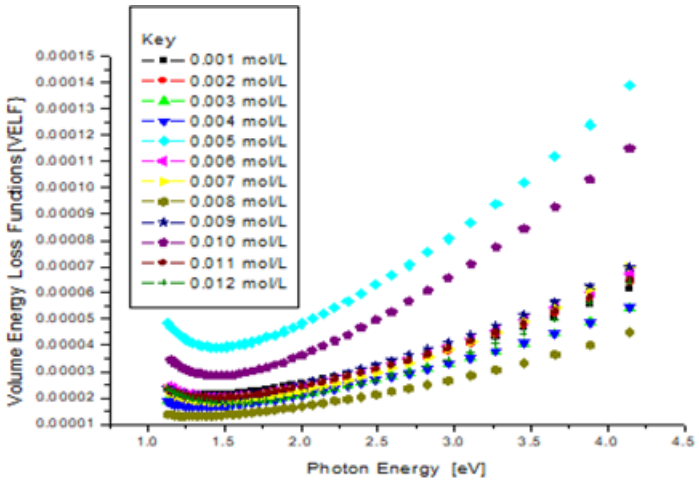

Figure 12: Plot of VELF against Photon Energy

Inter-band Transition Strength

Transition can describe a material with similar composition or uniform constituents (Yuan *et al.*, 2016), and, therefore, the quality of the material can be used. For example, total inter-band transition strength J_{cv} was determined, and Figure 13 shows how it varies with photon energy. Figure 13 also shows that the uniform J_{cv} can be attributed to inter-bands' closeness in the films.

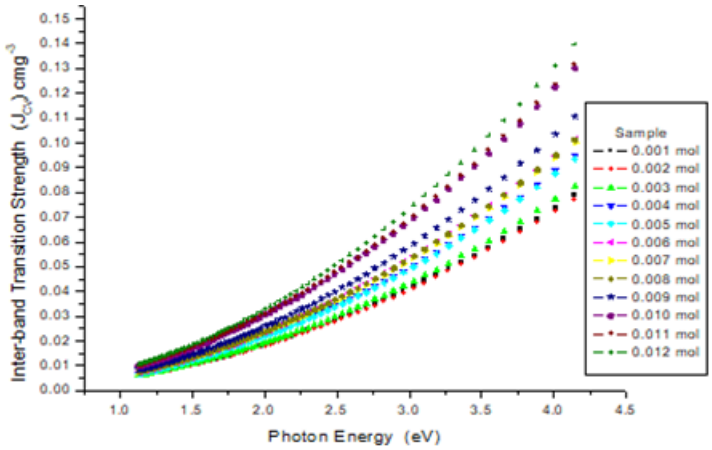

Figure 13: Plot of Inter-band transition strength against photon energy

It influences thickness, DOS (density of states), and optical density. As a result, more inter-bands come to populate closer and closer and finally get overpopulated. Due to overpopulation, the Moss Burstein effect causes band gap widening. Inter-band transition strength can be used to explain the trends in changes in the optical band gap of $CH_3NH_3PbI_3$ films with concentration. Figure 14 shows that inter-band transition strength is relatively constant compared to VELF, SELF, and band gap energy. Most of these energies have a relatively low but significant contribution to the band gap.

Inter-band transition strength depends on the sensitivity of band gap energy to changes in concentration and that transition strength. It influences spacing between the filled valances band and the empty of unfilled conduction bands. For the $CH_3NH_3PbI_3$ films, the transition energy was 1.741 eV, with VEL of 1.732 eV, E_g of 1.723 eV, and SEL of

1.711eV. Semi-classical Kane has previously studied interband tunneling through modeling (Nagabhushanaa *et al.*, 2016). When you apply the Kramers-Kronig model, a linear baseline exhibits the strength of natural interband transition. Any anomalous band gap intensities are removed by performing a fit using the power law (which may come about due to Urbach energy) that causes such unwanted offsets at the high point.

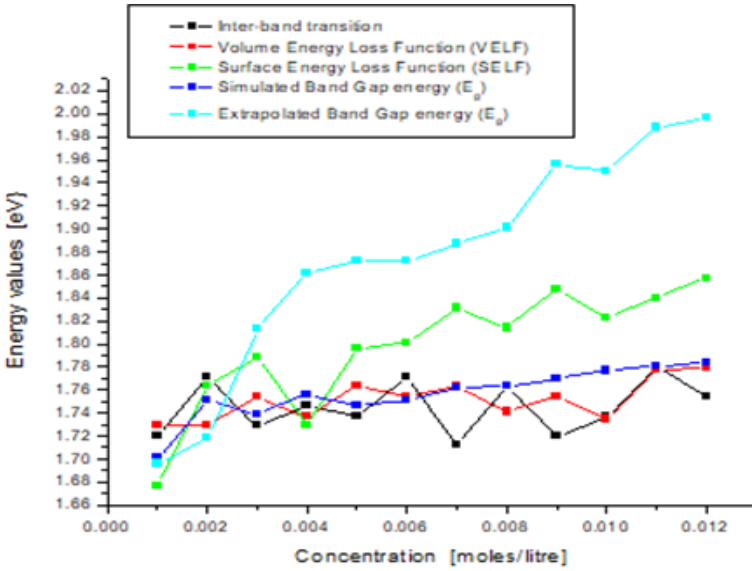

Figure 14: Comparison of VELF, SELF, Band Gap, and JCV energies

In most cases, using extrapolation when analyzing interband strength is not very appropriate. Instead, it extends transition energies beyond the energies that activate Qerenkov transition effects and radiation transition to set in or occur. It is believed that such an error might influence analysis to yield a linear baseline of interband strength (J_{cv}) going through exact the origin. This suggestion is still under fierce debate. It is argued that this approach neglects coupling that is expected to occur with other bands and causes an underestimation of transverse tunneling. Equally, the two-band Hamiltonian and the Kane analytical formula are widely used to determine interband tunneling by considering interband transition experience challenges when used along unconfined directions in nanostructures, especially in hybrid $CH_3NH_3PbI_3$ perovskites.

Nonlinear Optical Polarizability

To estimate the nonlinear optical polarizability effects in $CH_3NH_3PbI_3$ films, *Wemple-Didomenico* Model (Byung-wook *et al.*, 2015) was adopted. It combined with Miller's rule to analyze the visible and near-infrared frequencies within 300 - 1100 nm wavelength ranges. As proposed by Zhaoning *et al.* (2015), the third-order nonlinear polarizability parameter, $(\chi)^{(3)}$, depends almost entirely on a nonlinear optical susceptibility, and it is related by $(n^2 - 1)^{-4}$ to give $\chi^{(3)} \times 10^{-10}$ *esu* when plotted against wavelength (λ). Figure 15 shows the third-order nonlinear polarizability parameter, $(\chi)^{(3)}$ against concentration.

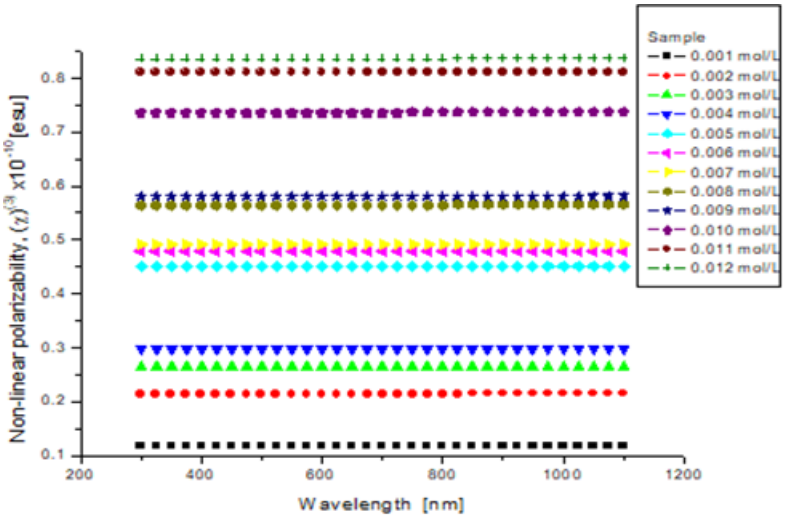

Figure 15: Plot of $(n^2 - 1)^{-4}$ or $\chi^{(3)}$versus wavelength

It was observed that nonlinear polarizability is influenced by concentration such that higher concentrations influence higher levels of nonlinear polarizability in $CH_3NH_3PbI_3$ films and that polarizability does not depend on photon energy. By implication, this further suggested that refractive index, dielectric constant, and polarizability also depend on the concentration. If they are nonlinear, their non-linearity should increase as wavelength approaches the absorption edge (*closer to where resonance conditions are met*) of the material in question.

CONCLUSION

In this paper, various internal energy components for $CH_3NH_3PbI_3$ films were investigated, analyzed, and reported findings. Analysis showed that the different types of internal energies influence the optical properties of $CH_3NH_3PbI_3$ films and significantly contribute to determining the application type for its layers. The simulation estimated inter-band transition energy of 1.741 eV, VEL of 1.732 eV, E_g of 1.722 eV, and SEL of 1.711eV for the $CH_3NH_3PbI_3$ as perovskite film layer that depended on band gap energy. The Urbach energy, VELF, and SELF energies influence electrical susceptibility. The dielectric constant plays a key role and is a functional energy storage property. Refractive index was found to determine the amount of energy absorbed by a perovskite just as earlier decided by Amgar *et al.* (2016), Mattoni *et al.* (2016), and Yuan *et al.* (2016), respectively. Therefore, a detailed study of $CH_3NH_3PbI_3$ thin film internal energies and how they influence optical properties provide helpful information to consider when designing a better optical device using $CH_3NH_3PbI_3$ perovskite films.

ACKNOWLEDGMENTS

The authors acknowledge the Department of Mathematics and Physics of the Technical University of Mombasa.

CONFLICT OF INTEREST

The author declares no conflict of interest with the Technical University of Mombasa or any other entity of persons.

REFERENCES

Amgar, D., Aharon, S., &Etgar, L. (2016). Inorganic and Hybrid Organo-Metal Perovskite Nanostructures: Synthesis, Properties, and Applications. *Advanced Functional Materials*, *26*(47), 8576-8593.

Arun, P., Jelissa, J., Vytenis, P.,Joël, T., and Jacques-E, M. (2015). Dynamics of photocarrier separation in $MAPbI_3$ perovskite multigrain films under a quasistatic electric field. *The Journal of Physical Chemistry C*, *120*, 19595−19602.

Byung-wook, P., Bertrand, P., Sagar, J., Xiaoliang, Z., Tomas, E., Hakan, R., Burkhard. Z. and Gerrit, B. (2015). Chemical engineering of methyl ammonium lead iodide/bromide perovskites: Tuning of optoelectronic properties and photovoltaic performance, *Journal of Materials Chemistry A, 3,* 21760–21771.

Chun-Sheng, J., Mengjin, Y., Yuanyuan, Z., Bobby, T., Sanjini, U. Joseph, M. Weilie, Z., Joseph J., Jao, L., Nitin,P. Padture, Kai Zhu1 & Mowafak M. Al-Jassim, (2015). Carrier separation and transport in perovskite solar cells studied by nanometre-scale profiling of electrical potential. *Nature Communications*, *6*, 8397. https://doi.org/10.1038/ncomms9397

Dalouji, V., Elahi, S., & Ahmadmarvili, A. (2017). Electric susceptibility and energy loss functions of carbon-nickel composite films at different deposition times. *Silicon*, ***9***(5), 717-722.

Edoardo M., Thibaud, E. and Filippo, A. (2016). First-principles modeling of organohalide thin films and interfaces, *Springer International Publishing*, *5,* 19-65.

Fan, P., Gu, D., Liang, G. X., Luo, J. T., Chen, J. L., Zheng, Z. H., & Zhang, D. P. (2016). High-performance perovskite $CH_3NH_3PbI_3$ thin films for solar cells prepared by single-source physical vapour deposition. *Scientific reports*, *6*, 29910.

Gogoi, P. K., & Schmidt, D. (2016). Temperature-dependent dielectric function of bulk $SrTiO_3$: Urbach tail, band edges, and excitonic effects. *Physical Review B*, *93*(7), 075204.

Gokmen, T., Gunawan, O., Todorov, T. K., & Mitzi, D. B. (2013). Band tailing and efficiency limitation in kesterite solar cells. *Applied Physics Letters*, *103*(10), 103506.

Gonzalez-Pedro, V., Juarez-Perez, E. J., Arsyad, W. S., Barea, E. M., Fabregat-Santiago, F., Mora-Sero, I., & Bisquert, J. (2014). General working principles of $CH_3NH_3PbX_3$ perovskite solar cells. *Nano letters*, *14*(2), 888-893.

Jun, Y., Daniele, C., Anurag, K. Shi, C., Nripan, M., Andrew, C. Grimsdale, and Cesare, S., (2015). Interfacial charge transfer anisotropy in polycrystalline lead iodide perovskite films, *Journal of Physical Chemistry Letters*, *6,* 1396−1402.

Kholmirzo, T., Sagille, A., Pavel, P., Anatoly V., Alexey R., Tatyana Y., (2015). Molecular dynamics simulations of perovskites: The effect of potential function representation on equilibrium structural properties, *Open Journal of Physical Chemistry, 5*, 110-121

Kim, J., Lee, S. H., Lee, J. H., & Hong, K. H. (2014). The role of intrinsic defects in methyl ammonium lead iodide perovskites. *The journal of physical chemistry letters*, *5*(8)

Laura M., (2016). Charge-carrier dynamics in organic-inorganic metal halide perovskites, *Annual* Review *of Physical Chemistry*, 67, 65–89.

Lee, Y., Kwon, J., Hwang, E., Ra, C. H., Yoo, W. J., Ahn, J. H., ... & Cho, J. H. (2015). High-performance perovskite graphene hybrid photo detector. *Advanced materials*, *27*(1), 41-46.

Lien, D., Anitha, E., Jo ,V. , Jean, M. , Edoardo, M. ,Filippo A., and Hans-Gerd, B, (2015). Intrinsic thermal instability of methyl ammonium lead trihalide perovskite, *Advanced Energy Materials, 5*(15), 1500477

Lindblad, R., Jena, N. K., Philippe, B., Oscarsson, J., Bi, D., Lindblad, A., ... & Siegbahn, H. (2015). Electronic structure of $CH_3NH_3PbX_3$ perovskites: dependence on the halide moiety. *The Journal of Physical Chemistry C*, *119*(4), 1818-1825.

Mariona C., Andrés, G., Elena, M., Osbel, A., Germa, G., Mariano, C., and Juan B., (2015). Polarization switching and light-enhanced piezoelectricity in lead (II) halide perovskites, The *Journal of Physical Chemistry Letters, 5,* 120-131. https://doi.org/10.1021/acs.jpclett.5b00502

Mattoni, A., Filippetti, A., & Caddeo, C. (2016). Modeling hybrid perovskites by molecular dynamics. *Journal of Physics: Condensed Matter*, *29*(4), 043001.

Men´endez-Proupin, E., Palacios, P., Wahn´on, P. and Conesa, C. (2014). Self-consistent relativistic band structure of the $CH_3NH_3PbI_3$ perovskite, *Physical Review B, 90*, 045207

Nadim, M., Mengjin, Y., Zhen, L., Nazifah, I., Xuan, K., and Zhaoyang, F. (2016). Polarization and dielectric study of methyl ammonium lead iodide thin film to reveal its nonferroelectric nature under solar cell operating conditions, *American Chemical Society Energy Letters, 1,* 142–149.

Nagabhushanaa, G., Radha, S., and Alexandra, N. (2016). Direct calorimetric verification of thermodynamic instability of lead halide hybrid perovskites. *Proceedings of the National Academy of Sciences, 113*(28), 7717–7721. https://doi.org/10.1073/pnas.1607850113

Sadhanala, A., Cacovich, S., Divitini, G., Vrućinić, M., Friend, R., Sirringhaus, H., Deschler, F. and Ducati, C. (2015). Nanoscale investigation of organic – inorganic halide perovskites. *Journal of Physics: Conference. 644***,** 012-024. https://doi.org/10.1088/1742-6596/644/1/012024

Simon, A., Jonas, W, James, A., and Lukas, S. (2015). Physical and electrical characteristics of lead halide perovskites for solar cell applications. *American Institute of Physics, 2,* 040701.

Valerio, A., Mingjian, Y., Riccardo, C., Emmanuel, S., Dong, S., Makhsud, I., Pongsakorn, K., Damir, K., Sjoerd, H., Zheng-Hong, L., Osman, M., and Edward, H. (2016). The In-Gap Electronic State Spectrum of Methyl ammonium Lead Iodide Single-Crystal Perovskites, Advanced *Materials, 28,* 3406–3410.

Vandewal, K., Benduhn, J., & Nikolis, V. C. (2018). How to determine optical gaps and voltage losses in organic photovoltaic materials. *Sustainable Energy & Fuels*, **2**(3), 538-544.

Wei, D., Ma, F., Wang, R., Dou, S., Cui, P., Huang, H., ... & Elseman, A. M. (2018). Ion-Migration Inhibition by the Cation $-\pi$ Interaction in Perovskite Materials for Efficient and Stable Perovskite Solar Cells. *Advanced Materials*, *30*(31), 1707583.

Yang, B., Brown, C. C., Huang, J., Collins, L., Sang, X., Unocic, R. R., ... & Geohegan, D. B. (2017). Enhancing ion migration in grain boundaries of hybrid organic–inorganic perovskites by chlorine. *Advanced Functional Materials*, *27*(26), 1700749.

Yani, C., Minhong, H., Jiajun, P., Yong, S., and Ziqi, L., (2016). Structure and growth control of organic–inorganic halide perovskites for optoelectronics: From polycrystalline films to single crystals. *Advanced Science*, **3,** 1500392.

Yuan, Y., Wang, Q., Shao, Y., Lu, H., Li, T., Gruverman, A., & Huang, J. (2016). Electric-field-driven reversible conversion between Methyl ammonium lead tri-iodide perovskites and lead iodide at elevated temperatures. *Advanced Energy Materials*, *6*(2), 1501803.

Zhaoning, S., Suneth, C., Adam, B., Brandon, L., Randy, J., and Michael, J., (2015). Impact of processing temperature and composition on the formation of methyl ammonium lead iodide perovskites, *Chemistry of Materials,* **27,** 4612–4619.

--0--